Theory and practice of interpolation in the pyramid domain

Antoine Guitton and Jon Claerbout

ABSTRACT

With the pyramid transform, 2-D dip spectra can be characterized by 1-D prediction-error filters (pefs) and 3-D dip spectra by 2-D pefs. This transform takes data from (ω, x)-space to data in $(\omega, u = \omega \cdot x)$-space using a simple mapping procedure that leaves empty locations in the pyramid domain. Missing data in (ω, x)-space create even more empty bins in (ω, u)-space. We propose a multi-stage least-squares approach where both unknown pefs and missing data are estimated. This approach is tested on synthetic and field data examples where aliasing and irregular spacing are present.

INTRODUCTION

For interpolation, it is often assumed that the seismic data are made from a superposition of locally planar events [Claerbout (1992); Symes (1994); Fomel (2002)]. Since plane-waves are highly predictable, interpolating seismic data with prediction-error filters (pefs) is both very effective and efficient, either in the Fourier [Spitz (1991)] or time domain [Crawley et al. (1999)].

In the Fourier domain and for aliased data, pefs from lower frequencies are used to de-alias higher frequencies [Spitz (1991)]. Therefore, many pefs need to be estimated for complete processing. Sun and Ronen (1996) introduce a frequency dependent sampling in the (ω, x) domain such that a data vector $\mathbf{d}$ at each frequency in the (ω, x) domain is mapped into a new vector $\mathbf{m}$ (pyramid domain) according to

$$m(\omega, u) = d(\omega, x = u/\omega), \tag{1}$$

where u has units of velocities and x is a spatial axis (offset or mid-point position). We demonstrate in this paper that this transform has the advantage of making the pefs frequency independent, thus offering useful properties (for stationary data):

- Only one pef is necessary for interpolation
- This single pef can be estimated from all the frequencies
- For noisy data, many regressions are available from all the frequencies, yielding robust pef estimation

This paper investigates the pyramid domain method and introduces a linear operator called the pyramid transform. First, we illustrate the properties of the pyramid transform and explain why, in theory, only one pef is necessary for interpolation. Second, we identify mapping artifacts from (ω, x)-space to $(\omega, u = \omega \cdot x)$-space and propose a strategy both to attenuate them and to interpolate seismic data. This strategy works for both aliased and irregularly-sampled data. Finally, we illustrate the proposed algorithm on synthetic and real data cases.

THEORY: INTRODUCING THE PYRAMID TRANSFORM

In this section, we first introduce the pyramid transform, which is a linear operation that remaps the Fourier transformed data in (ω, x) into the pyramid domain in (ω, u). Then we introduce some properties of the pyramid domain and their implications for pef estimation and missing data interpolation.

The pyramid transform

To begin introduce the forward transformation from the pyramid domain (ω, u) to the Fourier space (ω, x) as follows:

$$d(\omega, x) = m(\omega, u = \omega \cdot x). \tag{2}$$

The adjoint transformation is defined in equation (1). These definitions can be extended in 3-D easily for the forward case:

$$d(\omega, x, y) = m(\omega, u = \omega \cdot x, v = \omega \cdot y), \tag{3}$$

and for the adjoint case:

$$m(\omega, u, v) = d(\omega, x = u/\omega, y = v/\omega), \tag{4}$$

where y is a spatial axis in the crossline direction (offset of mid-point position) and v the dual of y in the pyramid domain. Equations (2) and (3) can be rewritten in a more compact form:

$$\mathbf{d} = \mathbf{L}\mathbf{m}, \tag{5}$$

where $\mathbf{L}$ is the pyramid transform. Similarly, equations (1) and (4) can be rewritten as

$$\mathbf{m} = \mathbf{L}'\mathbf{d}, \tag{6}$$

where $\mathbf{L}'$ is the adjoint of $\mathbf{L}$. Note that the remapping between x and u (plus y and v in 3-D) requires an interpolation operator. A linear interpolation process looping over the data space $d(\omega, x)$ is applied in all our results.

Properties

The equation of a plane-wave in (t, x) is given by

$$P(t, x) = f(t - px), \tag{7}$$

where f is a waveform and p is a constant slope. The prediction operator B from one trace to another at a distance Δx in (ω, x) for the plane-wave in equation (7) is given by Fomel (2002):

$$B(\omega, \Delta x) = e^{i\omega p \Delta x}. \tag{8}$$

If we now introduce the new variable $\Delta u = \omega \Delta x$ in equation (8), then we have a new prediction operator A in the (ω, u) domain:

$$A(\omega, \Delta u) = e^{ip\Delta u}. \tag{9}$$

From Equation (9), we notice that the dependency in ω of the prediction operator has vanished in the pyramid domain. Sun and Ronen (1996) extend this property to more than one plane-wave. We illustrate the pyramid domain in Figure 1. Figure 1a shows two plane-waves with the same wavelet (Ricker 2 with a fundamental frequency of 20Hz). Figure 1b displays the real part of the Fourier transformed data in the (ω, x) domain and Figure 1c the real part of the (ω, u) pyramid domain. Notice that we limited the range of frequencies for display purposes only in Figures 1b and 1c. In 2-D, the pyramid domain maps into a triangle-shaped area. In 3-D, it will map into a pyramid-shaped volume. Consequently, each trace in (ω, x) is transformed into a radial trace in (ω, u).

As anticipated from the definition of the prediction operator in equation (9), the information at each frequency in Figure 1c is independent of ω, which means that any scheme involving pefs in the pyramid domain will require only one filter (one 1-D filter for 2-D data, and one 2-D filter for 3-D data). In addition, we observe that the slope p now acts as a wavenumber on the u axis. This fact implies that the low velocity event in Figure 1a will look like a high wavenumber component on the u-axis whereas the high velocity event will look like a low wavenumber. An added feature is that since we only have one pef for the whole domain (in theory), the filter estimation should be relatively robust to the noise present in the data (especially for random noise).

Transformation artifacts

Going back and forth between the (ω, x) and (ω, u) domains will leave artifacts in (t, x). There are two main reasons for this. First, the linear interpolation operator we use to transform one domain to the other is not unitary. Second, the pyramid transform (forward and adjoint operators) compresses and stretches the horizontal axis in ways that can affect the reconstruction of the frequency content, especially for the low frequencies [remember that a trace in (ω, x)-space is mapped into a radial

trace in (ω, u)-space]. We illustrate this effect in Figure 2a. This Figure is the result of the following operation:

$$\tilde{\mathbf{d}} = \mathbf{L}\mathbf{L}'\mathbf{d} \tag{10}$$

where $\mathbf{d}$ is the Fourier transform of Figure 1a and $\tilde{\mathbf{d}}$ contains the reconstructed data. In this example, because the u axis is too coarse, the information of the slowest event (ringiest on the u axis) disappears.

In order to mitigate these effects, we propose making the u axis very dense. Theoretically, we could derive the maximum bin size δu to accommodate the slowest event. From simple Fourier analysis, we can establish that

$$\delta u \leq \frac{1}{2p_{max}}, \tag{11}$$

where p_{max} is the slope of the slowest event. This relation is a necessary, but not sufficient, condition for δu since some of the artifacts are also due to the linear interpolation itself (i.e., the linear interpolation operator is not unitary). Therefore in practice, smaller δu's than the one in equation 11 are necessary. Having very fine sampling in u will help attenuate most of the transformation errors seen in Figure 2. Figure 3 shows $\mathbf{L}\mathbf{L}'\mathbf{d}$ for the same dataset, but with a sampling 12 times finer on the u axis than on Figure 2b. Now, Figure 3a shows the two events with some remaining artifacts due to the linear interpolation operator only. In the next section, we introduce an algorithm that will both remove these remaining artifacts and also allow us to interpolate missing data.

ALGORITHM FOR MISSING DATA INTERPOLATION

Having a very fine sampling on the u axis attenuates most of the transformation artifacts of the pyramid transform. However, as seen in Figure 3a, some noise due to the linear interpolation operator used for the mapping between the (ω, x) and (ω, u) domains still remains. This section introduces an algorithm that will (1) remove the remaining artifacts and (2), interpolate missing data (regularly or irregularly spaced).

Mitigating mapping effects

The remaining artifacts in Figure 3a can be attenuated in many ways. For instance, Hung et al. (2004) propose using a sinc interpolation instead of a linear interpolation. Otherwise, if missing-data interpolation is not required, the effects of linear interpolation can be attenuated by inserting a tridiagonal solver within the adjoint in equations (1) and (4). Alternatively, we can recast this attenuation as an inverse problem, in which we want to minimize the energy of the residual vector $\mathbf{r}$ where

$$\mathbf{r} = \mathbf{L}\mathbf{m} - \mathbf{d}, \tag{12}$$

and minimize $f(\mathbf{m}) = \|\mathbf{r}\|_2$ iteratively to find the minimum $\tilde{\mathbf{m}} = (\mathbf{L}'\mathbf{L})^{-1}\mathbf{L}'\mathbf{d}$. The results of this iterative formulation can be seen in Figure 4: The plane-waves are recovered without any noise. Note that the iterative solution and the tridiagonal solver approach are equivalent. However, the missing data problem we are trying to solve makes the tridiagonal solver difficult to use.

Putting everything together

We are now ready to present the missing data interpolation algorithm. One side effect of the fine sampling of the u axis is that empty bins will appear in the pyramid domain. Missing data in $\mathbf{d}$ will add even more empty locations. We propose interpolating the missing data in $\mathbf{d}$ by filling the empty bins in $\mathbf{m}$. For this, we follow the approach of Claerbout and Fomel (2002). First, we want to honor the data where they are known by introducing the residual vector

$$\mathbf{r_d} = \mathbf{W_d}(\mathbf{Lm} - \mathbf{d}), \tag{13}$$

where $\mathbf{W_d}$ is a masking operator equal to unity where data are known, and zero where data are missing. Solving for $\mathbf{m}$ minimizing the amplitude of $\mathbf{r_d}$ only will not fill the empty bins. We need to add a regularization term that will enforce a certain multivariate spectrum to the vector $\mathbf{m}$:

$$\mathbf{r_m} = \mathbf{Am}, \tag{14}$$

where $\mathbf{A}$ is a pef in the model space. Assuming that the pef $\mathbf{A}$ is known, we can fill the empty locations in $\mathbf{m}$ by minimizing $f(\mathbf{m}) = \|\mathbf{r_d}\|_2 + \epsilon\|\mathbf{r_m}\|_2$, where ϵ is a balancing operator between data fitting and model space regularization.

There are two issues with this approach. The first issue is that the convergence towards a solution will be slow. To accelerate this process we introduce a new variable $\mathbf{q} = \mathbf{Am}$ and rewrite equations (13) and (14) as follows:

$$\begin{aligned} \mathbf{r_d} &= \mathbf{W_d}(\mathbf{LA^{-1}q} - \mathbf{d}) \\ \mathbf{r_q} &= \mathbf{q} \end{aligned} \tag{15}$$

We then minimize $f(\mathbf{q}) = \|\mathbf{r_d}\|_2 + \epsilon\|\mathbf{r_q}\|_2$ and compute $\tilde{\mathbf{m}} = \mathbf{A^{-1}}\tilde{\mathbf{q}}$, where $\tilde{\mathbf{q}}$ minimizes $f(\mathbf{q})$. The term $\mathbf{A^{-1}}$ is computed by applying a polynomial division to $\mathbf{q}$ which yields fast filling of the empty bins. Because $\mathbf{A}$ is a miminum-phase filter, the polynomial division is stable and will not cause the solution to blow-up. This preconditioning of the problem has been used in numerous geophysical problems [Clapp et al. (2004); Fomel and Guitton (2006); Herrmann et al. (2009)]. In practice, we set $\epsilon = 0$ and minimize $\mathbf{r_d}$ only [Trad et al. (2003); Guitton and Claerbout (2004)].

The second issue is that both $\mathbf{q}$ and $\mathbf{A}$ are unknown in equation (15). To circumvent this problem we bootstrap the pef estimation by first assuming that $\mathbf{A}$ is a 1-D gradient. To make sure that we can apply the polynomial division, we set the second

coefficient of the gradient to -0.96 instead of -1. We then minimize $f(\mathbf{q})$ with this first pef, find a new $\tilde{\mathbf{m}}$ and estimate a better pef $\mathbf{A}$ from it. Having a better pef, we can minimize $f(\mathbf{q})$ again:

$$
\begin{aligned}
&\mathbf{A} \leftarrow (1 - 0.96)^T \\
&\text{iterate } \{ \\
&\qquad \text{minimize } f(\mathbf{q}) \\
&\qquad \tilde{\mathbf{m}} \leftarrow \mathbf{A^{-1}}\tilde{\mathbf{q}} \\
&\qquad \text{estimate } \mathbf{A} \text{ from } \tilde{\mathbf{m}} \\
&\qquad \}
\end{aligned}
$$

We are essentially solving the non-linear problem in a step-wise fashion by keeping $\mathbf{A}$ constant within each non-linear loop. In practice, we notice that only 4 to 5 non-linear iterations are necessary to converge towards a pef that yields accurate interpolation of the missing data.

In the next section, we apply this algorithm to synthetic and field data examples in 2-D. We show that aliased and irregularly-sampled data can be interpolated.

EXAMPLES

Results in this section illustrate how the pyramid domain can be used to interpolate missing data. One interesting feature of the preceding algorithm is that no assumptions are made concerning the type of problem that can be tackled: here, we show interpolation results for aliased and irregularly-spaced data.

Interpolation of aliased data

We illustrate in Figure 5 the dealiasing properties of the interpolation algorithm. Figure 5a shows an aliased dataset (Δx=50 m) as a first example. Its FK spectrum is displayed in 5b and illustrates the aliasing effects above 13 Hz. We interpolate this data set on a 25 m grid by first binning the data in Figure 5a onto a 25 m grid. This binning will leave every other trace empty: the weighting operator $\mathbf{W_d}$ in equation (15) is set to zero at these locations. Figures 5c and 5d display the interpolated data in (t, x) and (f, k)-spaces. Most of the aliasing has been removed, except for the slowest event. We completely de-alias this dataset by binning Figure 5c on a 12.5 m grid and interpolating the missing traces in the pyramid domain. This final interpolation is shown in Figures 5e and 5f.

Now, we interpolate non-stationary data for two shots from one synthetic and one field experiment. Being a frequency domain approach, the interpolation in the pyramid domain forces us to decompose the data in patches, or time windows, first. The size of these windows is one second in time and 500 m in offset. Each window is

processed independently. Figure 6a shows the input data for the synthetic example with a 50 m offset sampling. Its amplitude FK spectrum is displayed in Figure 6b: some events are aliased for frequencies above 15 Hz. After interpolation on a 25 m grid in Figure 6c, most of the aliased energy is gone (Figure 6d), while all the main events are preserved. Note that in principle, more interpolation steps would be necessary to remove all aliased energy (above 30 Hz).

Finally, we interpolate a shot gather from a field data experiment in the Gulf of Mexico (Figure 7). The close-up in Figure 7a shows primaries above 4 seconds and multiples below. The FK spectrum in Figure 7b shows some aliasing for the slowest events around 40 Hz. We interpolate this shot from a 26 m to a 13 m grid in Figure 7c. Most of the aliasing artifacts have been attenuated (Figure 7d).

Interpolation of irregularly-sampled data

The interpolation of irregularly-sampled data in the pyramid domain requires a binning of the data onto a regular grid first. This binning is done with a simple nearest-neighbor scheme. Like what is done for the regular case, the weighting operator $\mathbf{W_d}$ in equation (15) is set to zero at the empty trace locations. For all following examples, 50% of the traces were set to zero randomly in order to emulate a realistic acquisition geometry.

Figure 8a shows the data to interpolate with its amplitude spectrum (Figure 8b). Many methods exploit the FK domain directly in order to interpolate missing data [Xu et al. (2005); Abma and Kabir (2006); Zwartjes and Sacchi (2007)], with or without nonuniform Fourier transforms. The interpolation result in Figure 8c proves that the proposed algorithm works in this case as well. The FK domain in Figure 8d validates these findings.

Figure 9a and 9c display the input data and the interpolation results, respectively. This dataset is similar to the one used in Figure 6a. The missing traces have been properly interpolated almost everywhere. Where gaps are big, however, the proposed algorithm might have some difficulties which could be overcome by using a multi-scaling strategy. Note, in Figures 9b and 9d, the clean up of the FK domain after interpolation.

Finally, we interpolate irregularly-spaced data for a field data example shown in Figure 10a. This dataset was also used in Figure 7a. Like what we observed in the previous example, the interpolation result in Figure 10c exemplifies how the proposed algorithm can interpolate missing data: the reconstructed traces look very similar to the original ones. The FK spectra in Figures 10b and 10d show the attenuation of artifacts due to the random sampling in Figure 10a.

Parameter estimation

One of the most important parameters in our algorithm is the sampling in the pyramid domain. We find that for interpolating irregularly-spaced data, half of the value of δu given in equation 11 is usually enough. For interpolating aliased data, however, the sampling becomes more difficult to establish. In this case, the sampling becomes smaller as the maximum non-aliased frequency becomes smaller. In practice, we tend to find the right sampling by trial and error, starting from the value we would use for the irregularly-spaced data case. This approach is unsatisfying and we feel that more work should be done to automate this important parameter selection.

CONCLUSION

The pyramid transform creates a domain where linear events in (t, x)-space are linear in (ω, u)-space. This property offers many opportunities for interpolation schemes based on prediction-error filters. First, one filter can predict all frequencies. Second, this pef can be estimated from all frequencies. Finally, the filter estimation should be more robust to the noise present in data (although not shown here).

One challenge with the pyramid transform is the remapping between the (ω, x) and (ω, u) domains which can introduce artifacts. We propose mitigating these effects by making the pyramid axis u very dense and using a simple linear interpolation for the transform. One consequence of this proposal is that many empty bins appear in the pyramid domain. Realizing that missing data will add even more empty locations, we introduce a non-linear algorithm that both interpolates missing data (regularly or irregularly-spaced data) and fills the empty bin locations (those resulting from the transform).

Our synthetic and field data experiments prove that the proposed algorithm works and that the pyramid domain is a sensible complement to our existing interpolation toolbox. Although not presented here, the extension to 3-D would be straightforward. Interpolating aliased or irregularly-space data does not require any change of the algorithm. However, we notice that smaller δu's are required when de-alasing is needed.

Comparing the pyramid transform to other domains for missing data interpolation goes beyond the scope of this paper, but more work needs to be done to understand how the proposed algorithm fairs when compared to more popular techniques such as FX interpolation.

The pyramid transform could benefit other applications. For instance, the irregular sampling case could be treated with a combination of nonuniform Fourier transform and pyramid transform. The signal/noise separation problem could be easily recast in the pyramid domain where only 1-D (for 2-D data) and 2-D (for 3-D data) projection filters are necessary [Soubaras (1994)].

ACKNOWLEDGMENTS

We thank Shuki Ronen and Xukai Shen for numerous discussion on this topic. We also thank the sponsors of the Stanford Exploration Project for their financial support.

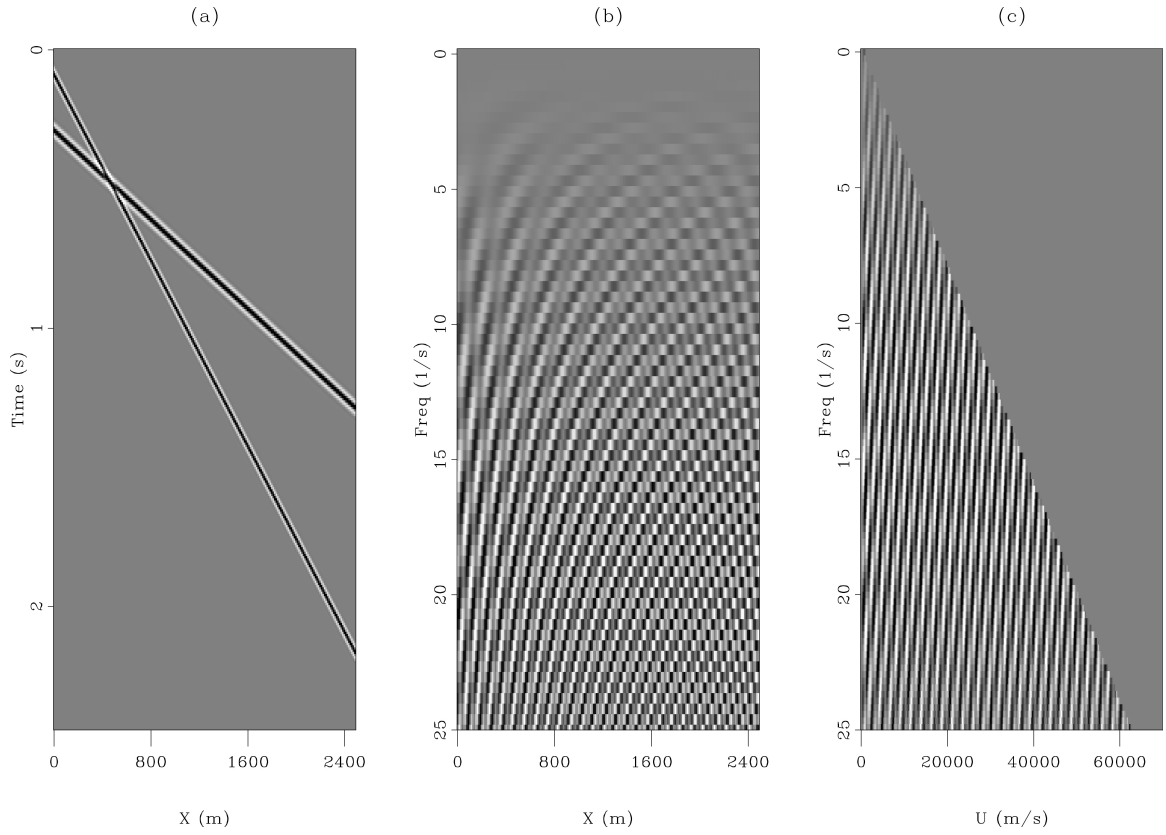

Figure 1: Two plane waves in (a) (t, x), (b) (ω, x) and (c), (ω, u) domains.(b) and (c) show the real parts only. **[NR]**

REFERENCES

Abma, R. and N. Kabir, 2006, 3D interpolation of irregular data with a POCS algorithm: Geophysics, **71**, E91–E97.

Claerbout, J., 1992, Earth Sounding Analysis, Processing versus Inversion: Blackwell Scientific Publications.

Claerbout, J. and S. Fomel, 2002, Image Estimation by Example: Geophysical Soundings Image Construction: Class notes, http://sepwww.stanford.edu/sep/prof/index.html.

Clapp, R. G., B. L. Biondi, and J. F. Claerbout, 2004, Incorporating geologic information into reflection tomography: Geophysics, **69**, 533–546.

Crawley, S., R. Clapp, and J. Claerbout, 1999, Interpolation with smoothly nonstationary prediction-error filters: SEG Technical Program Expanded Abstracts, **18**, 1154–1157.

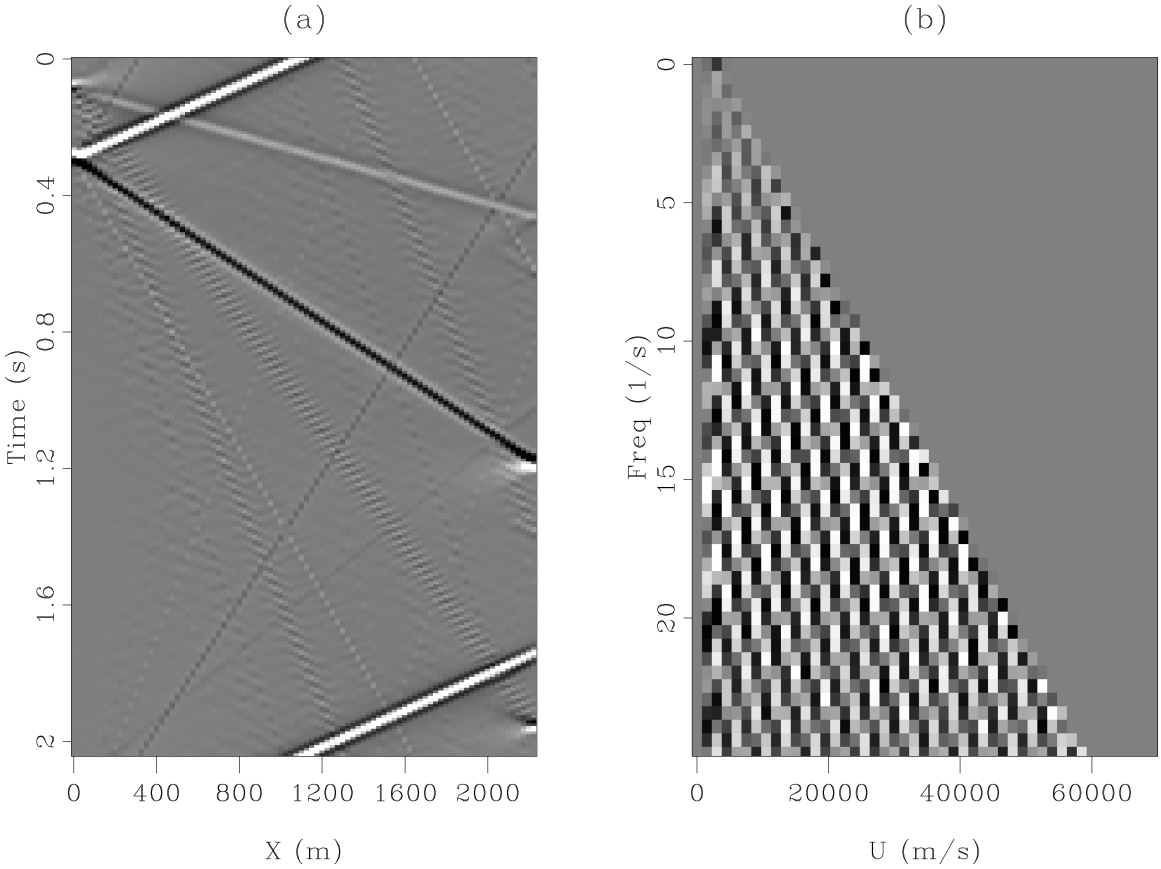

Figure 2: Illustration of transformation artifacts: (a) is $\mathbf{LL'd}$ back in the (t, x) domain and (b) is the real part $\Re(\mathbf{L'd})$, where $\mathbf{d}$ is the data in Figure 1a. The slowest event, with the highest wavenumber component on the u axis, disappears due to the parameterization of the pyramid transform. **[NR]**

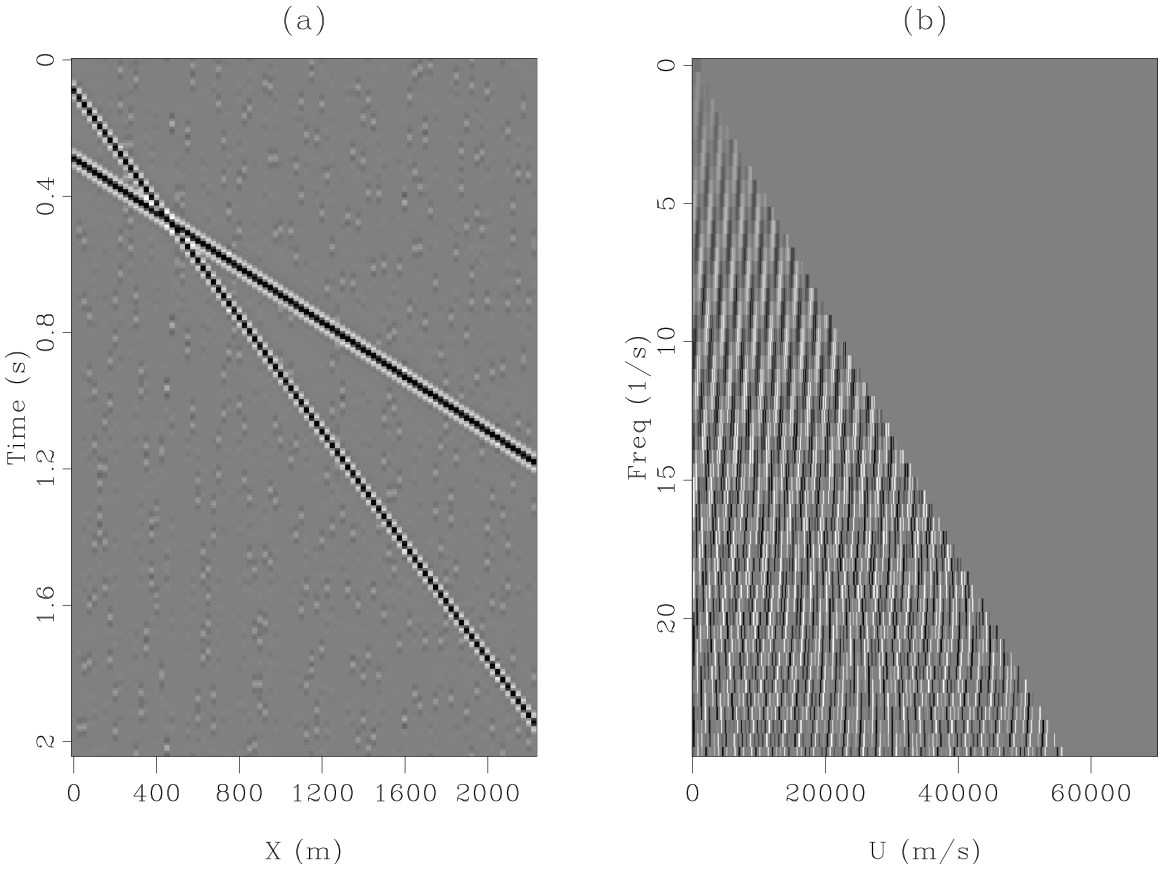

Figure 3: Same as Figure 2 but with a 12 times finer horizontal sampling on the u axis. The two plane-waves are recovered. Some noise is still present due the linear interpolation operator. **[NR]**

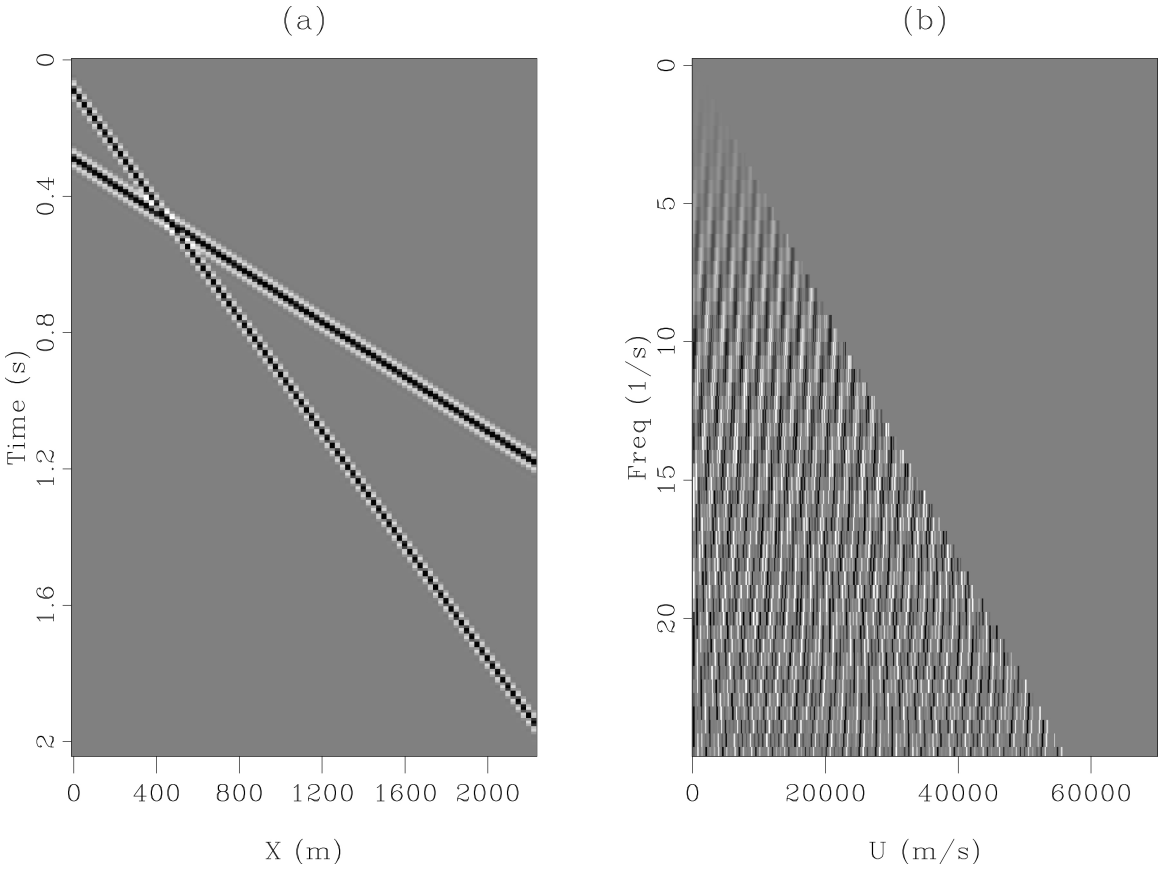

Figure 4: Illustration of the iterative process to attenuate the effects of linear interpolation. (a) is $\mathbf{L}\tilde{\mathbf{m}} = \mathbf{L}(\mathbf{L}'\mathbf{L})^{-\mathbf{1}}\mathbf{L}'\mathbf{d}$ back in the (t, x) domain and (b) is $\Re(\tilde{\mathbf{m}})$. The noise in Figure 3a has been attenuated. **[NR]**

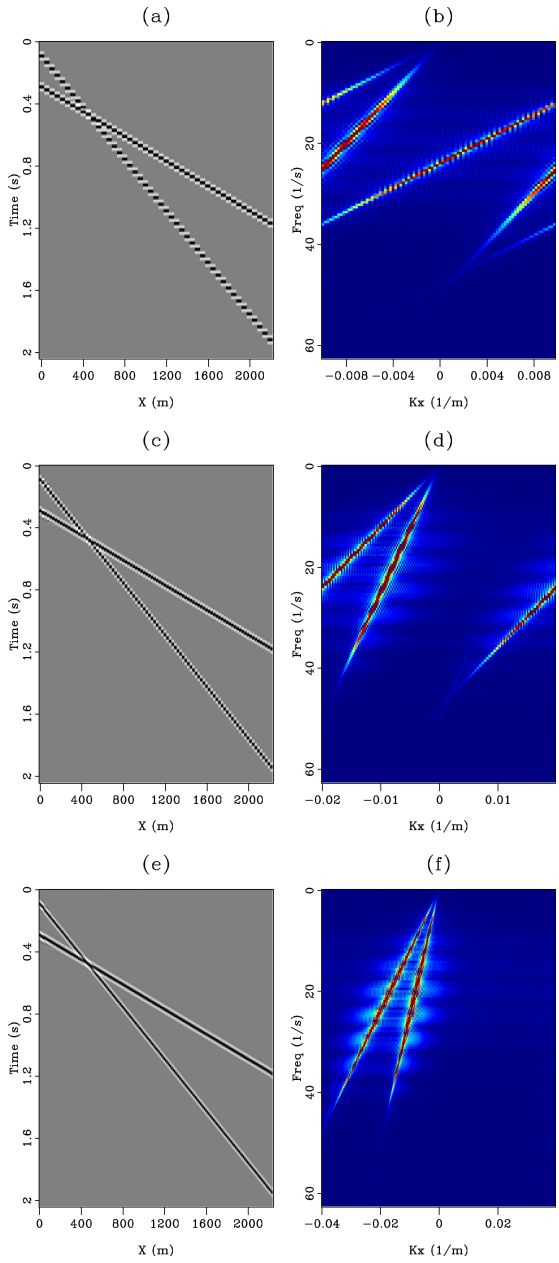

Figure 5: Interpolation results for aliased data: (a) Shows the input data at Δx=50 m and its corresponding FK spectrum in (b). The slowest event is aliased for frequencies above 13 Hz and the fastest for frequencies above 22 Hz. (c) Shows the interpolation result with Δx=25 m and the corresponding FK spectrum in (d). The slowest event is still aliased above 22 Hz. (e) Shows the interpolation result with Δx=12.5 m and the corresponding FK spectrum in (e). The data in (a) have been dealiased for all frequencies. [**NR**]

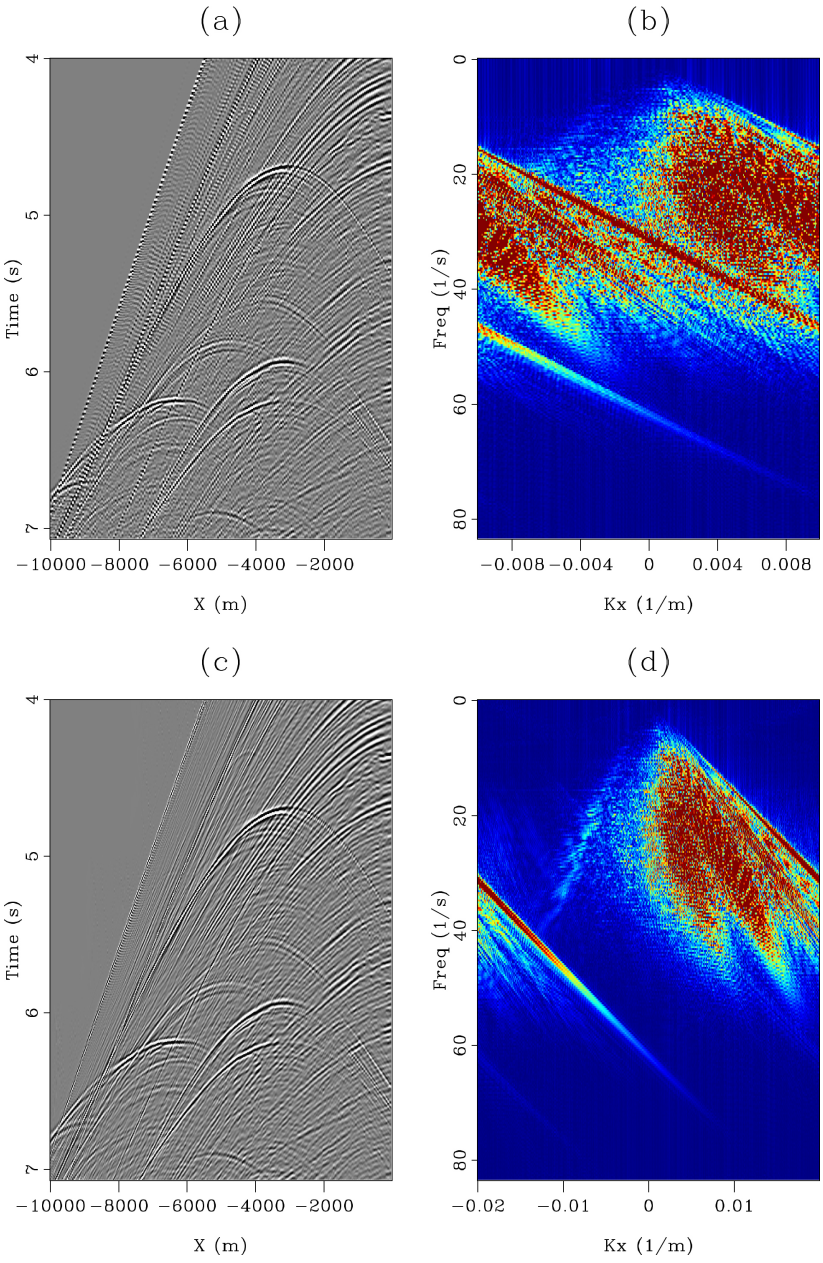

Figure 6: Interpolation results of a realistic synthetic data experiment. (a) Shows the input data on a 50 m grid with its FK amplitude spectrum in (b). (c) Shows the same data after interpolation on a 25 m grid (FK spectrum in (d)). All the events have been correctly interpolated but some aliasing remains. **[NR]**

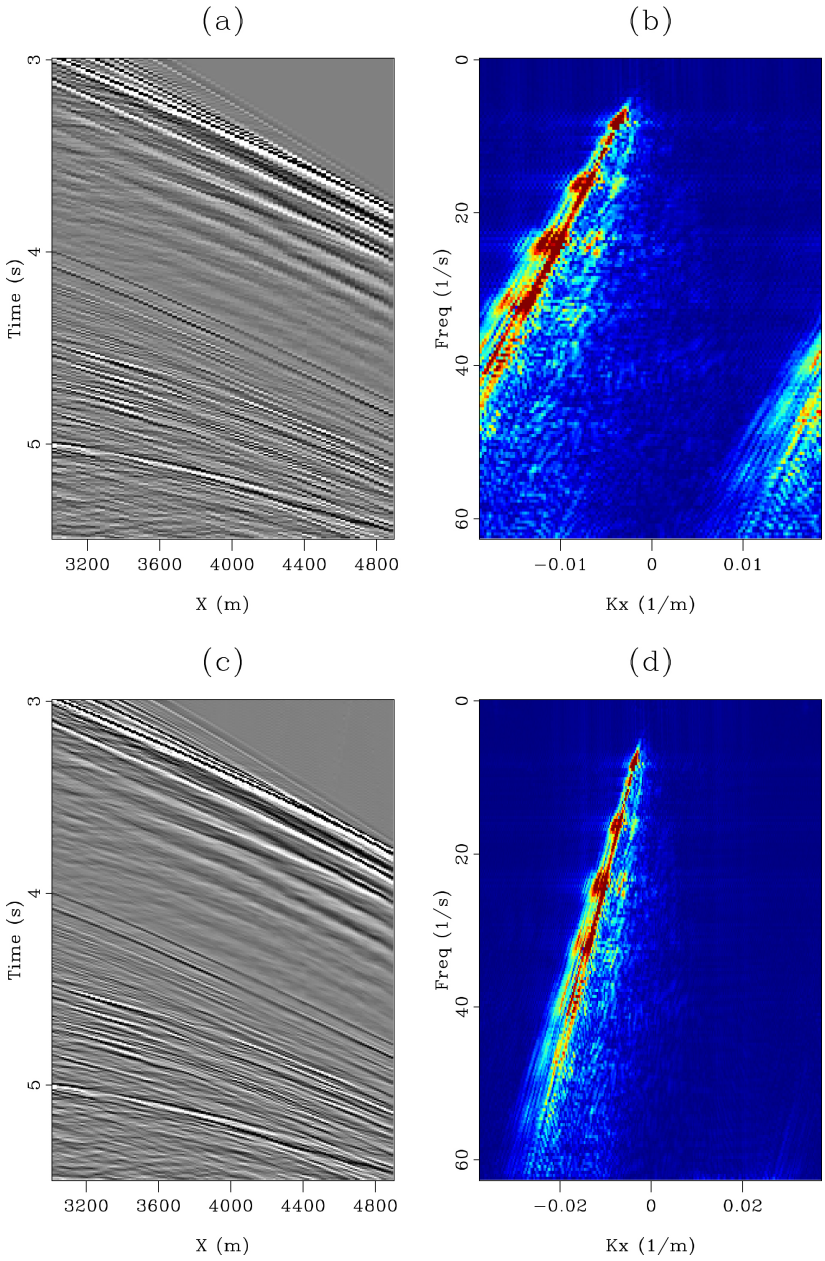

Figure 7: Interpolation results of a shot gather from the Gulf of Mexico. (a) Shows a close-up of the input data on a 26 m grid with its FK amplitude spectrum in (b). (c) Shows the same data after interpolation on a 13 m grid (FK spectrum in (d)). All the events have been correctly interpolated. [**NR**]

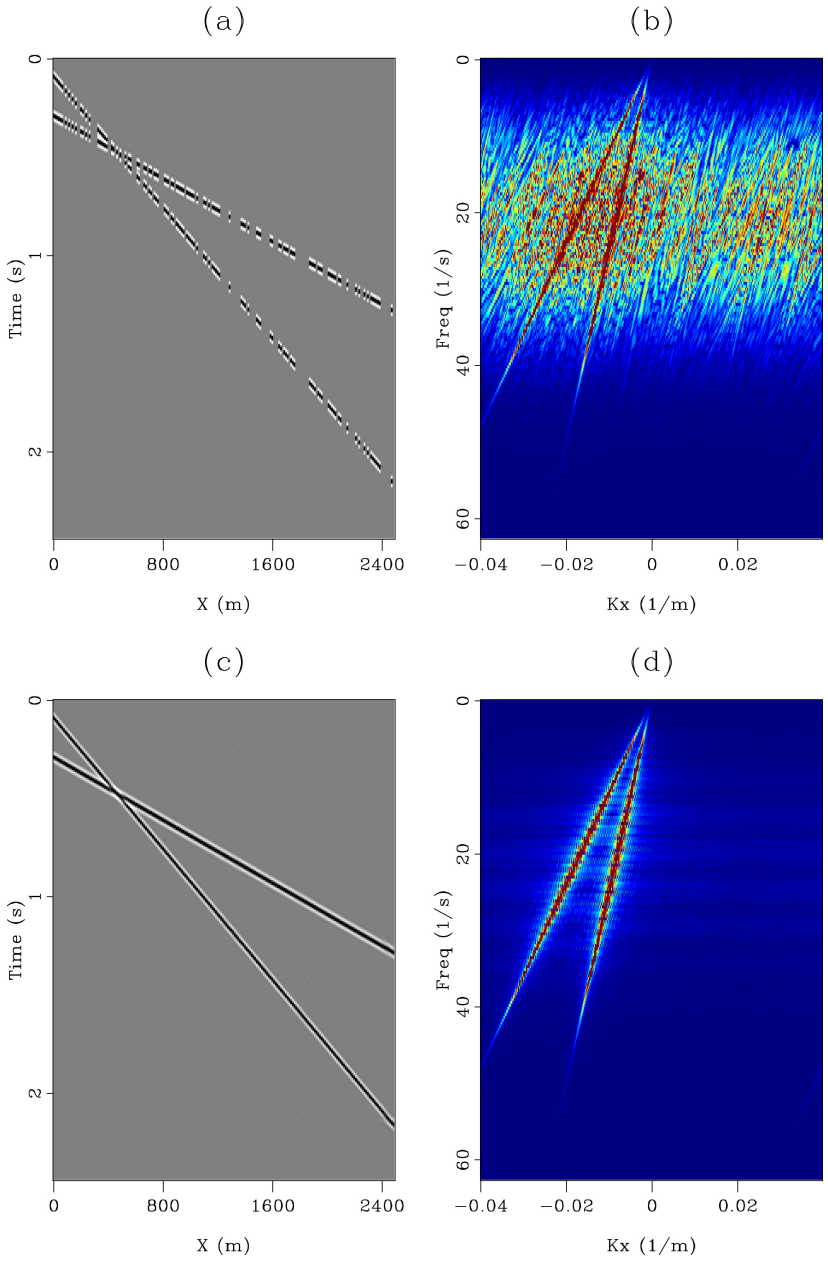

Figure 8: Interpolation of irregularly-sampled data. (a) Shows the input data binned onto a regular grid before interpolation where 50% of the traces are missing and its corresponding FK spectrum in (b). Interpolation results are shown in (c) (FK spectrum in (d)): the linear events are recovered. **[NR]**

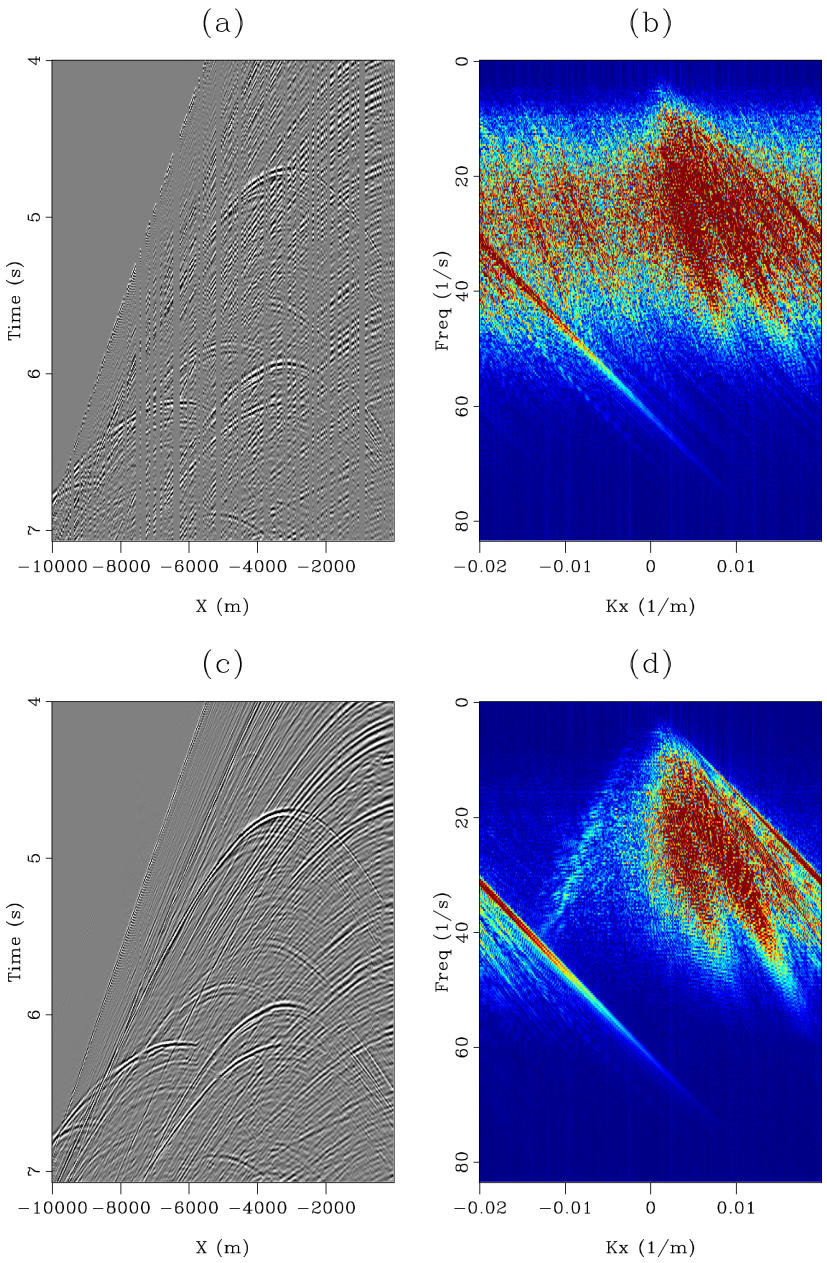

Figure 9: Interpolation of a synthetic shot gather with irregular sampling. (a) Shows the input data binned onto a regular grid before interpolation and its corresponding FK spectrum in (b). Interpolation results are shown in (c) (FK spectrum in (d)). Our proposed algorithm recovers the missing traces where conflicting dips are present. **[NR]**

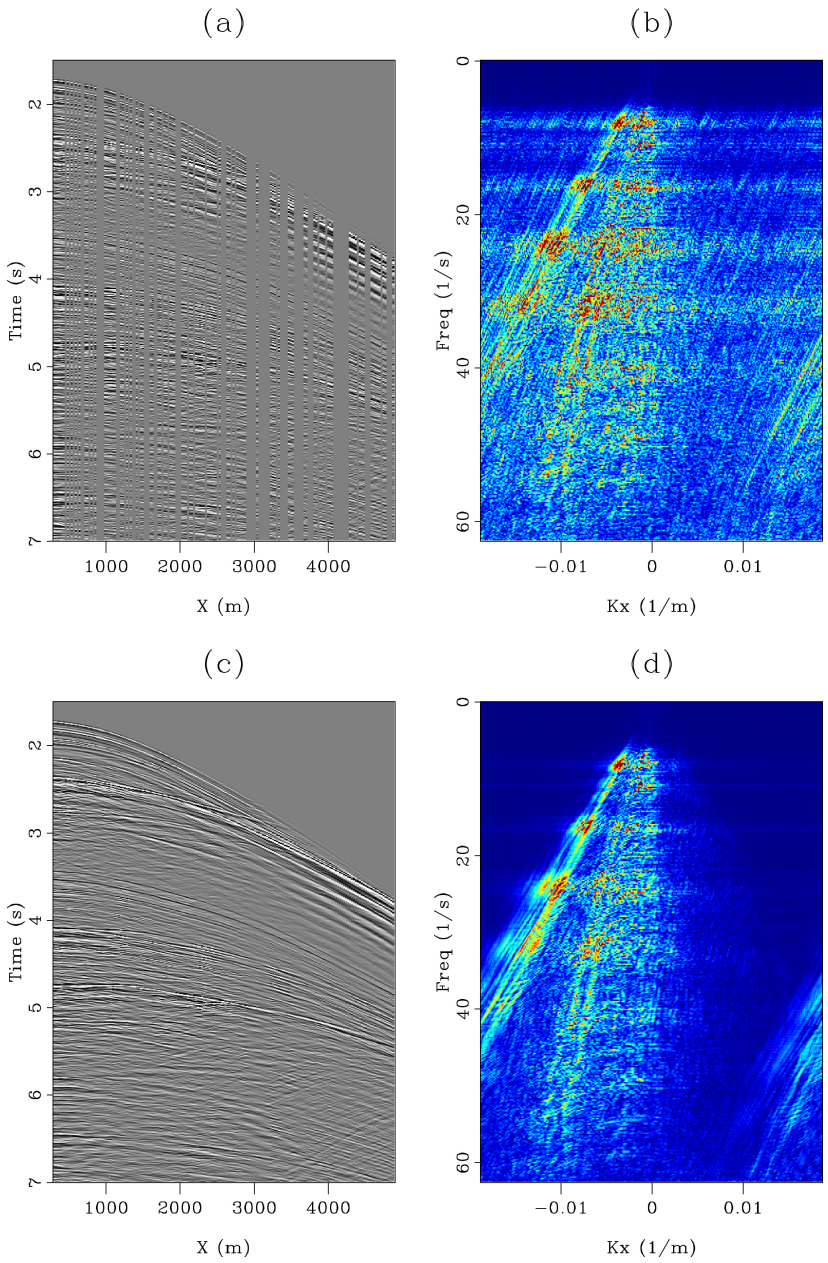

Figure 10: Interpolation of a shot gather from the Gulf of Mexico with irregular sampling. (a) Shows the input data binned onto a regular grid before interpolation and its corresponding FK spectrum in (b). Interpolation results are shown in (c) (FK spectrum in (d)). The missing traces are reconstructed and there is no noticeable footprint left by the interpolation algorithm. [**NR**]

Fomel, S., 2002, Applications of plane-wave destruction filters: Geophysics, **67**, 1946–1960.

Fomel, S. and A. Guitton, 2006, Regularizing seismic inverse problems by model reparameterization using plane-wave construction: Geophysics, **71**, A43–A47.

Guitton, A. and J. Claerbout, 2004, Interpolation of bathymetry data from the Sea of Galilee: A noise attenuation problem: Geophysics, **69**, 608–616.

Herrmann, F. J., C. R. Brown, Y. A. Erlangga, and P. P. Moghaddam, 2009, Curvelet-based migration preconditioning and scaling: Geophysics, **74**, A41–A46.

Hung, B., C. Notfors, and S. Ronen, 2004, Seismic trace interpolation using the pyramid transform: SEG Technical Program Expanded Abstracts, **23**, 2017–2020.

Soubaras, R., 1994, Signal-preserving random noise attenuation by the F-X projection: SEG Technical Program Expanded Abstracts, **13**, 1576–1579.

Spitz, S., 1991, Seismic trace interpolation in the F-X domain: Geophysics, **56**, 785–794.

Sun, Y. and S. Ronen, 1996, The pyramid transform and its application to signal/noise separation: SEP-Report, **93**, 161–176.

Symes, W. W., 1994, The plane-wave detection problem: Inverse Problems, **10**, 1361–1391.

Trad, D., T. Ulrych, and M. Sacchi, 2003, Latest views of the sparse Radon transform: Geophysics, **68**, 386–399.

Xu, S., Y. Zhang, D. Pham, and G. Lambaré, 2005, Antileakage Fourier transform for seismic data regularization: Geophysics, **70**, V87–V95.

Zwartjes, P. M. and M. D. Sacchi, 2007, Fourier reconstruction of nonuniformly sampled, aliased seismic data: Geophysics, **72**, V21–V32.